Effect of γ −Al 2 O 3 /Water Nanofluid on Heat Transfer and Pressure Drop Characteristics of Shell and Coil Heat Exchanger With Different Coil Curvatures

ARTICLE · DECEMBER 2015

DOI: 10.1115/1.4030635

4 AUTHORS:

Mohamed Reda Salem
Benha University
3 PUBLICATIONS **0** CITATIONS
SEE PROFILE

Ragab Khalil Ali
Benha University
13 PUBLICATIONS **6** CITATIONS
SEE PROFILE

Ramadan Sakr
Benha University
19 PUBLICATIONS **8** CITATIONS
SEE PROFILE

Karam El-Shazly
Benha University
11 PUBLICATIONS **15** CITATIONS
SEE PROFILE

Effect of γ-Al_2O_3/Water Nanofluid on Heat Transfer and Pressure Drop Characteristics of Shell and Coil Heat Exchanger With Different Coil Curvatures

M. R. Salem
Mechanical Engineering Department,
Faculty of Engineering at Shoubra,
Benha University,
108 Shoubra Street, Cairo 11629, Egypt
e-mails: me_mohamedreda@yahoo.com;
mohamed.abelhamid@feng.bu.edu.eg

R. K. Ali
Mechanical Engineering Department,
Faculty of Engineering at Shoubra,
Benha University,
108 Shoubra Street, Cairo 11629, Egypt
e-mail: ragabkhalil1971@gmail.com

R. Y. Sakr
Mechanical Engineering Department,
Faculty of Engineering at Shoubra,
Benha University,
108 Shoubra Street, Cairo 11629, Egypt
e-mail: rsakr85@yahoo.com

K. M. Elshazly
Mechanical Engineering Department,
Faculty of Engineering at Shoubra,
Benha University,
108 Shoubra Street, Cairo 11629, Egypt
e-mail: drkaramelshazly@yahoo.com

This study presents an experimental investigation of the characteristics of convective heat transfer in horizontal shell and coil heat exchangers in addition to the friction factor for fully developed flow through their helically coiled tube (HCT). Five heat exchangers of counterflow configuration were constructed with different HCT-curvature ratios (δ) and tested at different mass flow rates and inlet temperatures of γ-Al_2O_3/water nanofluid in the HCT. The tests were performed for γ-Al_2O_3 with average size of 40 nm and particles volume concentration (φ) from 0% to 2% for $0.0392 \leq \delta \leq 0.1194$. *Totally, 750 test runs were performed from which the HCT-average Nusselt number ($\overline{Nu}_t$) and fanning friction factor (f_c) were calculated. Results illustrated that $\overline{Nu}_t$ and f_c of nanofluids are higher than those of the pure water at same flow condition, and this increase goes up with the increase in φ. When φ increases from 0% to 2%, the average increase in $\overline{Nu}_t$ is of 59.4–81% at lower and higher HCT-Reynolds number, respectively, and the average increase in f_c is of 25.7% and 27.4% at lower and higher HCT-Reynolds number, respectively, when φ increases from 0% to 2% for $\delta = 0.1194$. In addition, results showed that $\overline{Nu}_t$ and f_c increase by increasing coil curvature ratio. When δ increases from 0.0392 to 0.1194 for $\varphi = 2\%$, the average increase in $\overline{Nu}_t$ is of 130.2% and 87.2% at lower and higher HCT-Reynolds number, respectively, and a significant increase of 18.2–7.5% is obtained in the HCT-fanning friction factor at lower and higher HCT-Reynolds number, respectively. Correlations for $\overline{Nu}_t$ and f_c as a function of the investigated parameters are obtained.* [DOI: 10.1115/1.4030635]

Keywords: heat exchanger, nanofluid, helically coiled tube, curvature, friction

1 Introduction

Most of heat transfer enhancement methods are limited by inherent restriction of thermal conductivity of the conventional fluids that are required for high-performance cooling or heating processes [1–3]. One of the ways to overcome this problem is to replace the conventional fluids with some advanced fluids with higher thermal conductivities. The key idea is to exploit the very high thermal conductivities of solid particles that can be several hundreds of times greater than all of the conventional fluids combined [4].

In most of the industrial applications, increasing the thermal performance of heat exchangers affects directly on energy, material, and cost savings. The major challenge in designing heat exchangers is to make the equipment compact and achieve a high heat transfer rate with minimum pumping power [5]. Coiled tubes of helical shape are one of the enhancement techniques that are widely used as heat exchangers and have applications in various industries: chemical, biological, petrochemical, mechanical, biomedical, and others. This wide using of HCTs is because they are compact and promote good mixing of the fluids that increasing the heat transfer coefficients. In addition, this equipment is low cost and of easy construction and maintenance [5–7]. Due to the extensive application of the HCTs in these fields, knowledge about the heat transfer and pressure drop characteristics is very important.

There are several studies in the literature concerning the friction losses due to flowing base fluids in HCTs [8–17]. These studies reported that an increase in the flow resistance compared with straight tubes. This is due to the centrifugal force caused by the pipe curvature. Correlations were obtained as a function of Re_t, δ, and Dean number (De). De is a dimensionless group that measures the ratio of the geometric average of inertial and centrifugal forces to the viscous forces, defined according to Eq. (1) in which Re_t is the HCT-Reynolds number based on axial flow velocity. Since the secondary flow is induced by centrifugal forces and their interaction primarily with viscous forces, De becomes a general measure of the magnitude of the secondary flow.δ is a dimensionless coil curvature ratio; it is the ratio of the inner diameter of the HCT ($d_{t,i}$) to the mean diameter of the coil curvature (D_c)

$$De = Re_t \delta^{0.5} \tag{1}$$

Kumar et al. [18] carried out an experiment on a shell and coil heat exchanger using nonmetallic sisal nanofluid ($\varphi \leq 0.5\%$). They reported that the overall heat transfer coefficient increased with increasing φ. It should be noted that their study did not account the effect of δ in calculation. Huminic and Huminic [19] numerically studied the heat transfer behavior of CuO/water and TiO_2/water nanofluids flowing through a counterflow double tube helical heat exchanger under laminar flow condition. The average

Contributed by the Heat Transfer Division of ASME for publication in the Journal of Thermal Science and Engineering Applications. Manuscript received May 7, 2014; final manuscript received March 31, 2015; published online June 9, 2015. Assoc. Editor: Mehmet Arik.

diameter of nanoparticles was about 24 nm and φ varied between 0.5% and 3%. Results showed that the use of nanofluids significantly enhances the convective heat transfer and the enhancement increases with De and φ.

Hashemi and Akhavan-Behabadi [20] experimentally studied the heat transfer and pressure drop characteristics of CuO (50 nm, 0.5–2 wt.%)/oil nanofluid flow inside horizontal HCT under laminar flow with constant heat flux. Observations showed that the heat transfer coefficient as well as pressure drop is increased by using nanofluid instead of base fluid. A maximum increase of 18.7% in heat transfer coefficient for $10 \leq \mathrm{Re_t} \leq 100$ was obtained for the straight tube, while an increase of 30.4% was obtained for the HCT, respectively, at the same $\mathrm{Re_t}$ range.

Kannadasan et al. [21–24] experimentally studied the heat transfer and pressure drop of γ-Al_2O_3 (0.1, 0.4, and 0.8 vol.%)/water nanofluid in HCT of shell and coil heat exchanger. The experiments were carried out using only one heat exchanger geometry in horizontal and vertical positions, in addition to counter and parallel flow configurations for $1600 < \mathrm{De} < 2700$ and $5200 < \mathrm{Re_t} < 8600$. The findings indicated that there is no considerable effect on $\overline{\mathrm{Nu}_\mathrm{t}}$ by changing flow configuration. It was shown also a considerable increase in the convective heat transfer coefficient and pressure drop with increasing φ. Compared to using pure water, an average increase in $\overline{\mathrm{Nu}_\mathrm{t}}$ and f_c was of 45% and 21%, respectively, in horizontal position, while the average increase in vertical position was of 49% and 25%, respectively.

Numerically and experimentally, Akbaridoust et al. [25] investigated the pressure drop and the convective heat transfer behavior of laminar CuO (68 nm, 0.1 and 0.2 vol. %)/water nanofluid flow in HCTs at a constant wall temperature. Results showed that more enhanced heat transfer is observed for HCTs as δ increased. In addition, utilization of base fluid in HCTs with greater δ compared to the use of nanofluid in straight tubes enhanced heat transfer more effectively. Aly [26] numerically studied the heat transfer and pressure drop characteristics of γ-Al_2O_3 ($\varphi \leq 2\%$)/water nanofluid flowing inside coiled tube-in-tube heat exchangers. Results showed that the heat transfer coefficient increases by increasing φ at the same $\mathrm{Re_t}$ or De. Moreover, the friction factor increases with the increase in δ and pressure drop penalty is negligible with increasing φ.

Elsayed et al. [27] presented a numerical study to investigate the combined effect of using helical coils and nanofluids on the heat transfer characteristics and pressure losses in turbulent flow regime. One uniformly heated HCT was used with λ of 0.0266 and δ of 0.0524. Results showed that combining the effects of γ-Al_2O_3 nanoparticles and tube coiling enhance the heat transfer coefficient by up to 60% compared with that of pure water in straight tube at the same $\mathrm{Re_t}$. Also, results showed that the pressure drop in HCTs using γ-Al_2O_3 ($\varphi = 3\%$)/water nanofluid is six times that of water in straight tubes (80% of the pressure drop increase is due to nanoparticles addition).

The present study aims to investigate experimentally the effect of γ-Al_2O_3 ($\varphi \leq 2\%$)/water nanofluid on characteristics of convective heat transfer in horizontal shell and coil heat exchangers with different coil curvatures over a wide range of HCT-fluid operating conditions. Present measurements are utilized to introduce experimental correlations for the HCT-average Nusselt number and fanning friction factor as a function of HCT-Reynolds number, Prandtl number, and coil curvature ratio.

2 Experimental Setup

The experimental facility employed in the present investigation consists of heating and cooling units, shell and coil heat exchanger, pumps, measuring devices, valves, and the connecting pipes. As illustrated in Fig. 1, each circuit contains bypass line and ball valve to control the mass flow rate directed to the heat exchanger. Two identical flow meters (1.7–18 l/min) were used to measure the volume flow rates directed to the test section. Twenty eight k-type thermocouples of 0.1 mm diameter were installed within each test section to measure the temperatures. Four thermocouples were inserted into the flow streams, at approximately 60 mm from the heat exchanger ports, to measure the inlet and exit temperatures of the shell and HCT fluids.

Twenty thermocouples were used to measure the HCT wall surface temperatures. They were mounted at ten equally distanced (441.5 mm) positions on the HCT surface, with installing two thermocouples at each position on the outer and inner diameter of the coil. To achieve higher accuracy in calculation of flow rate, four thermocouples were installed at inlet and exit of flow meters to record the flow temperature. All thermocouples were connected to a digital thermometer indicator with resolution of 0.1 °C to display the thermocouples outputs. A digital differential pressure transducer was employed for measuring the pressure drop of the pure water or γ-Al_2O_3/water nanofluid across the HCT. Two identical 1.5 hp rated power centrifugal pumps were installed to circulate the hot and cold liquids. Flexible nylon and polyvinyl chloride (PVC) tubes were used for all connections.

Figure 2 represents a photograph of the present setup. Two cylindrical containers of 50 l made of stainless steel (2 mm wall thickness) were employed as hot and cold fluid tanks. Each tank was installed inside 2 mm thick galvanized steel tanks with 20 mm gap, which was injected by polyurethane spray foam insulation to minimize the heat loss or gain. An electric heater of 6 kW rated power was fixed horizontally at the bottom of the heating tank to heat the pure water or γ-Al_2O_3/water nanofluid to the required temperature. The heat was removed from the water in the cooling tank by two cooling units of 10.5 kW cooling capacity. Sometimes the two cooling units operate in series, and in other times, in parallel manner to prevent thermal overloads. The operations of the electric heater and the cooler were based on pre-adjusted digital thermostats, which were used to keep constant temperatures of the liquids directed to both sides of the heat exchanger.

Five configurations of shell and coil heat exchanger were constructed with different HCT-curvature ratios. Due to the variation of curvature ratio ($\delta = d_{t,i}/D_c$), the coil pitch (p_c) and consequently number of turns (N) are varied to sustain constant coil torsion ratio ($\lambda = p_c/\pi D_c$) of 0.0895. The dimensions of the copper tube used in each coil are 4.415 m lengths, 9.52 mm outer diameter, and 8.3 mm inner diameter. The characteristic dimensions of the different configurations are revealed in Table 1. A photograph and schematic diagram of the shell and coil heat exchanger are shown in Fig. 3.

The shell of the heat exchangers was made of mild steel (2 mm wall thickness) and was formed as cylindrical shape. Two nipples of same material and 4 mm wall thickness were welded on both ends of the shell. The inlet and exit ports of the shell where pipes of constant cross section (100 mm length and 50.8 mm internal diameter) were welded to the shell. The distance between these ports centers and the neighboring shell end was 50 mm, which made the HCT partially block the opening as recommended by Kupprn [28]. Ten holes of 1 mm diameter were made in the shell wall to pass the thermocouples to their positions on the HCT surface. The holes were drilled directly facing the positions of the thermocouples to provide the smallest length of the thermocouples in the shell to minimize their effect on the shell flow. Moreover, outer surface of the shell was thermally isolated with thick insulation using a layer of each of ceramic fiber, asbestos rope, and glass wool. Finally, all equipments were assembled: the shell and coil heat exchanger, heating and cooling units, pumps, ball valves, connecting lines, and the measuring devices.

3 Nanofluids Preparation

Preparing stable suspension of nanoparticles in the base liquid was the first step in applying nanofluids as a heat transfer working fluid. The particles used in the nanofluid experiments are gamma-alumina (γ-Al_2O_3) nanopowders, supplied by Inframat® Advanced Materials Corporation, Manchester, CT (99.99% purity, product code 26 N-0801 G, 40 nm average particle size with

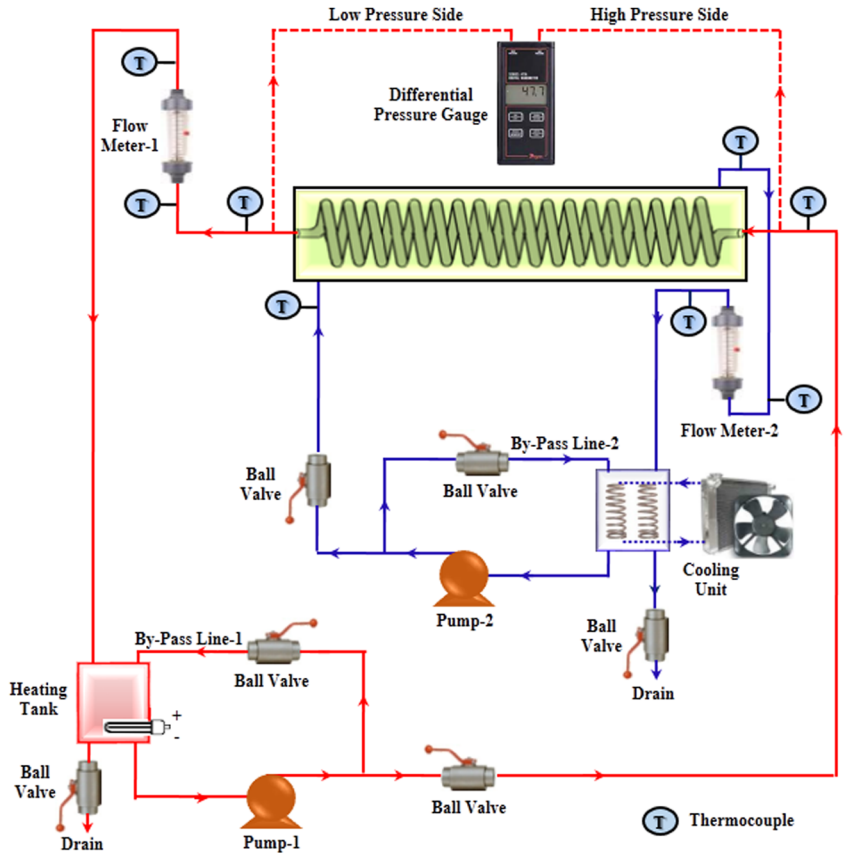

Fig. 1 Schematic diagram of the experimental apparatus

Fig. 2 A photograph of the experimental apparatus

surface area > 200 m^2/g). The thermophysical properties of γ-Al_2O_3 nanoparticles are revealed in Table 2.

The γ-Al_2O_3/water nanofluid was prepared in this study with four different nanoparticles volume concentrations of 0.5%, 1%, 1.5%, and 2%. The dispersion of particles in water was done by mixing the required particle volume concentration in the measuring flask. Agitator bath generating 3450 rpm was switched on for 18 hrs daily for two sequential days to get the uniform dispersion and stable suspension. In addition, to achieve good mixing for the nanofluid in the heating tank, the nanofluid was pumped in the HCT for 2 hrs before beginning the experiments. Furthermore, the bypassed line tube was extended to the bottom of heating tank. This tube has closed end while the side surface has numerous small holes, which act as nozzles to avoid any settlement of nanoparticles. It was observed with naked eyes that there was no significant settlement of nanoparticles for first six days of static condition of nanofluid. Nevertheless, settlement appeared gradually from the seventh day and the complete settlement occurred after 13 days. This is revealed in Fig. 4 for $\varphi = 2\%$.

Of course, this is one of the disadvantages of nanofluids, but it should be noted that the 13 days are in static conditions, and during operation there is no any settlement. In addition, it was seen that after settlement, the remixing process is very easy and requires smaller time and power to reproduce good mixture.

Table 1 Characteristic dimensions of the used shell and coil heat exchangers

HCT no.	D_c (mm)	δ	p_c (mm)	$it\lambda$	L_{sh} (mm)	$D_{sh,i}$ (mm)	$D_{sh,h}$ (mm)	N
1	69.5	0.1194	19.52	0.0895	505	271	205.1	20.21
2	105.0	0.0790	29.52					13.38
3	140.5	0.0591	39.52					10.00
4	176.0	0.0472	49.52					7.98
5	211.5	0.0392	59.52					6.64

a) Photograph of the test section (shell and coil heat exchanger)

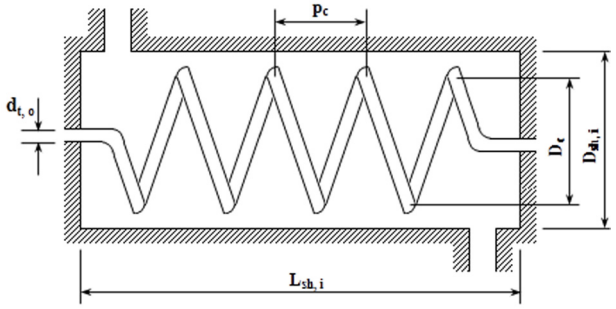

b) Schematic diagram of the shell and coil heat exchanger

Fig. 3 (*a*) A photograph and (*b*) schematic diagram of the test section

Table 2 Properties of γ-Al_2O_3 nanoparticles

Thermal conductivity (W/m °C)	Density (kg/m^3)	Specific heat (J/kg °C)
36	3600	773

Additionally, there are surfactants that help in increasing the suspension period of nanoparticles. Here, they were not used because they affect the thermophysical properties of nanofluids and the present research aims to study the effect of using pure nanofluid.

4 Experimental Procedures and Data Reduction

The first step in collecting data from the system was to fill the heating tank with pure water or nanofluid, which was prepared with the required nanoparticles concentration. The cooling tank was filled with water from the local water supply. Then, the heater, the cooling units, and the pumps were turned on. Inlet temperatures of both sides of the heat exchanger were adjusted by regulating the temperatures of the heating and cooling tanks through their thermostats. The flow rates were adjusted through the flow meters and the installed valves, which were regulated to obtain the required flow rates in the primary lines and the remainder is bypassed to the tanks. The range of the operating conditions is given in Table 3.

Table 3 Range of operating conditions

Parameters	Range or value
HCT-side nanofluid flow rate (l/min)	1.7–11.158
HCT-side nanofluid inlet temperature (°C)	45, 55, 65
Nanoparticles volume concentration (%)	0, 0.5, 1, 1.5, 2
Shell-side water flow rate (l/min)	6.018
Shell-side inlet temperature (°C)	20

During the operation, the steady state condition is conducted when the maximum variation of 0.5 °C for each thermocouple reading within 20 min. It should be noted that for heat transfer calculations, the fluid properties of the shell and HCT sides were calculated at the bulk temperatures, $T_{sh,m}$ and $T_{t,m}$, respectively. While for pressure drop calculations, the HCT water properties were calculated at the film temperature, T_f, as recommended by Schmidt [29]. The bulk and film temperatures are calculated as follows:

$$T_{sh,m} = (T_{sh,i} + T_{sh,o})/2 \tag{2}$$

$$T_{t,m} = (T_{t,i} + T_{t,o})/2 \tag{3}$$

$$\bar{T}_{t,s} = \frac{\sum T_{t,s}}{20} \tag{4}$$

$$T_f = (T_{t,m} + \bar{T}_{t,s})/2 \tag{5}$$

The inner surface temperature of the HCT wall was taken equal to outer surface due to very low conduction resistance of the tube wall. The water thermophysical properties were evaluated from Remsburg [30]. For γ-Al_2O_3/water nanofluid, the thermophysical properties were calculated using the following equations [31–34]:

$$k_{nf} = k_{bf}\left[\frac{k_{np} + 2k_{bf} + 2\varphi(k_{np} - k_{bf})}{k_{np} + 2k_{bf} - \varphi(k_{np} - k_{bf})}\right] + 5 \times 10^4 \xi \Gamma \varphi \rho_{bf} C_{p}bf \sqrt{\frac{\kappa T}{\rho_{np} d_{np}}} \tag{6}$$

$$\Gamma = (1722.3\varphi - 134.63) - (6.04\varphi - 0.4705)T \tag{7}$$

$$\xi = 0.0017(100\varphi)^{-0.0841} \tag{8}$$

Fig. 4 Photographs of the observed nanoparticles settlement ($\varphi = 2\%$)

$$\mu_{nf} = \frac{\mu_{bf}}{[1-\varphi]^{2.5}} + 5 \times 10^4 \xi \Gamma \varphi \rho_{bf} \sqrt{\frac{it\kappa T}{\rho_{np} d_{np}}} \tag{9}$$

$$\rho_{nf} = \varphi \rho_{np} + (1-\varphi)\rho_{bf} \tag{10}$$

$$C_p nf = \frac{\varphi(\rho_{np} C_p np) + (1-\varphi)(\rho_{bf} C_p bf)}{\rho_{nf}} \tag{11}$$

$$Pr_{nf} = \frac{\mu_{nf} C_p nf}{k_{nf}} \tag{12}$$

The measurements of the flow rates and inlet and outlet temperatures of both streams of the heat exchanger were used to calculate heat transfer rates on the HCT and shell sides (Q_t and Q_{sh}) as follows:

$$Q_t = \dot{m}_t C_p t(T_{t,i} - T_{t,o}) \tag{13}$$

$$Q_{sh} = \dot{m}_{sh} C_p sh(T_{sh,o} - T_{sh,i}) \tag{14}$$

Without heat gain or loss from the heat exchanger, there is an energy balance between the two streams ($Q_t = Q_{sh}$). In the real experiments, there would always be some discrepancy between the two heat transfer rates. Therefore, the arithmetical average of the two, Q_{ave}, can be used as the heat load of the exchanger. For all experimental tests, the heating and cooling loads calculated from the hot and cold sides did not differ by more than ±1.8%.

$$Q_{ave} = \frac{|Q_t| + |Q_{sh}|}{2} \tag{15}$$

The heat load of the heat exchanger, Q_{ave}, was used to calculate the average heat transfer coefficient for the HCT-side fluid, $\bar{h}_t$, and then the average Nusselt number for the HCT-side fluid, $\overline{Nu}_t$, as follows:

$$Q_{ave} = \bar{h}_t A_{t,i}(T_{t,m} - \bar{T}_{t,s}) \tag{16}$$

$$\overline{Nu}_t = \frac{\bar{h}_t d_{t,i}}{k_t} \tag{17}$$

HCT-Reynolds number can be written as follows:

$$Re_t = \frac{4\dot{m}_t}{\pi d_{t,i} \mu_t} \tag{18}$$

The overall thermal conductance was calculated from the temperature data and flow rates using Eq. (19) as follows:

$$U_o A_{t,o} = \frac{Q_{ave}}{\Delta T_{L.M}} \tag{19}$$

$$\Delta T_{L.M} = \frac{(T_{t,i} - T_{sh,o}) - (T_{t,o} - T_{sh,i})}{\ln\left[\frac{T_{t,i} - T_{sh,o}}{T_{t,o} - T_{sh,i}}\right]} \tag{20}$$

The fanning friction factor for the fluid in circulation inside the HCT, f_c, was calculated with the following equation:

$$f_c = \frac{\Delta P_c d_{t,i}}{2 L_t \rho_t u^2} = \frac{\Delta P_c \pi^2 \rho_t d_{t,i}^5}{32 L_t \dot{m}_t^2} \tag{21}$$

Daily and Harleman [35] reported that the developed region in HCTs may be along a distance equal to 50 diameters of the HCT. Also, Nigam et al. [36] presented that the fully developed region in HCTs is formed after a distance equal to 30 diameters of the HCT. These values represent 5.64–9.4% of the total length of the HCTs used in the present study, which can be neglected and the fully developed profiles are confirmed.

5 Uncertainty Analyses

In general, the accuracy of the experimental results depends on the accuracy of the individual measuring instruments and techniques. It should be noted that according to the manufacturer, uncertainty in the HCT outer and inner diameters is ±0.01 mm, which can be neglected. The uncertainty in the measured coil and shell dimensions was assumed to be ±0.5 mm; this was guessed quantity from meter scale. In addition, the uncertainty applied to the thermal properties of water was assumed to be ±0.1%. The uncertainty is calculated based upon the root sum square combination of the effects of each of the individual inputs as introduced by Kline and McClintock [37]. For all experimental runs, the uncertainty in Re_t was ±1.7%. Also, the average uncertainty was ±7% in $\overline{Nu}_t$ and ±3.7% in f_c.

6 Results and Discussions

First, the experimental apparatus and procedures were validated by comparing the results of $\overline{Nu}_t$ for water flowing through the HCT with $\overline{Nu}_t$ reported from literature. From the literature review, it is obvious that there is lack in the correlations required to calculate the heat transfer coefficient for applied shell and coil heat exchangers. On the contrary, there are a number of correlations in the literature for the $\overline{Nu}_t$ for water flowing through the HCT with isoflux and isothermal wall boundary conditions. Here, the present experimental data for $\overline{Nu}_t$ were validated with the experimental data obtained by Rogers and Mayhew [12], and Xin and Ebadian [38]. In addition, another comparison of the experimental data for HCT-fanning friction factor with the results of White [39] and Prasad et al. [10] was performed. The results of these comparisons are shown in Fig. 5. From this figure, it can be seen that the experimental results for both heat transfer and friction factor calculations are in good agreement with previous studies.

6.1 Heat Transfer Results. A series of 750 experiments were carried out on the five heat exchangers shown in Table 1, which were constructed with different coil curvature ratios. These configurations were tested at different mass flow rates and inlet temperatures for the HCT-side as presented in Table 2. Figure 6 illustrates $\overline{Nu}_t$ versus HCT-Reynolds number for $0 \le \varphi \le 2\%$ at $T_{t,i} = 55\,^{\circ}C$ and $\delta = 0.0591$ as a sample of the results.

It can be seen that $\overline{Nu}_t$ of nanofluids is higher than that of the base fluid at same flow condition, and this enhancement increases with the increase in φ. At lower and higher HCT-Reynolds number, the average increase in $\overline{Nu}_t$ is of 12.2% and 13.7%, respectively, at $\varphi = 0.5\%$ and of 59.4–81%, respectively, at $\varphi = 2\%$ for $\delta = 0.1194$. While its corresponding average increase for $\delta = 0.0392$ is of 22.8% and 14.3%, respectively, at $\varphi = 0.5\%$ and

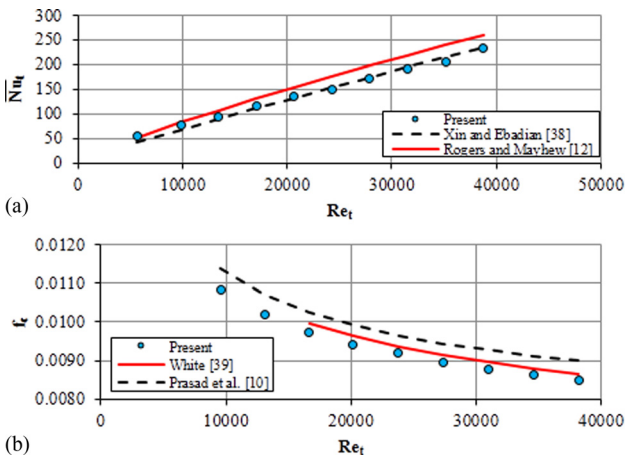

Fig. 5 Validation of the experimental data for HCT ($\lambda = 0.0895$)

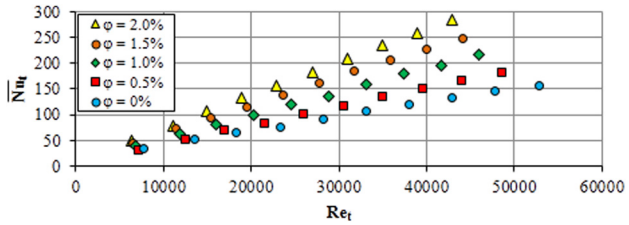

Fig. 6 Variation of HCT-average Nusselt number with HCT-Reynolds number at different nanoparticles concentrations ($T_{t,i} = 55\,^{\circ}C$, $\delta = 0.0591$)

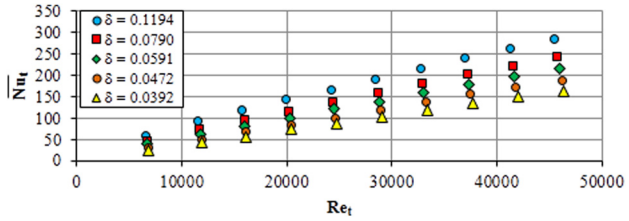

Fig. 7 Variation of HCT-average Nusselt number with HCT-Reynolds number at different HCT-curvature ratios ($\varphi = 1\%$, $T_{t,i} = 55\,^{\circ}C$)

of 81–74.1%, respectively, at $\varphi = 2\%$. This shows that enhancing heat transfer rates through using nanofluids as a thermal-fluid medium can be used to overcome poor heat transfer performance of pure water. Besides the enhanced thermal conductivity of nanofluids, the interactions and Brownian motion of nanoparticles and the resulting disturbance of the boundary layer may be responsible for the observed enhancement of heat transfer coefficients of nanofluids.

The influence of coil curvature on the thermal performance of the heat exchanger is studied for $0.0392 \leq \delta \leq 0.1194$. A sample of the results is shown in Fig. 7 for $\varphi = 1\%$ and $T_{t,i} = 55\,^{\circ}C$.

It is obvious that increasing coil curvature ratio increases the HCT-average Nusselt number. At lower and higher HCT-Reynolds number, the average increase in $\overline{Nu}_t$ is of 133.3% and 77.4%, respectively, at $\varphi = 0.5\%$, and of 130.2% and 87.2, respectively, at $\varphi = 2\%$, when the coil curvature ratio increases from 0.0392 to 0.1194. This can be attributed to the increase in the centrifugal force with higher coil curvature ratio, which induces more effective secondary flow. Also, it is clear that increasing HCT-Reynolds number increases the HCT-average Nusselt

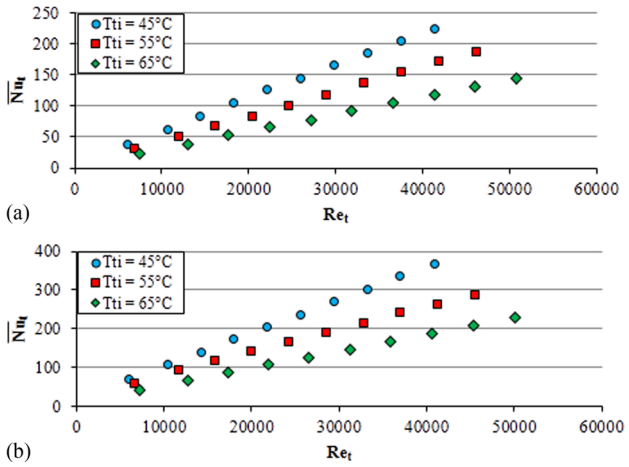

Fig. 8 Variation of HCT-average Nusselt number with HCT-Reynolds number at different HCT-inlet temperatures ($\varphi = 1\%$): (*a*) $\delta = 0.0472$ and (*b*) $\delta = 0.1194$

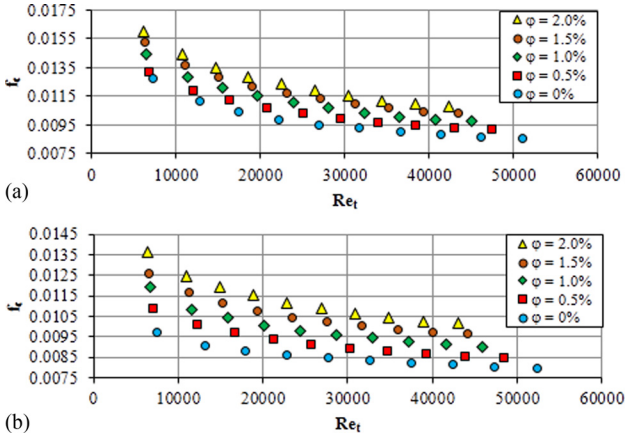

Fig. 9 Variation of HCT-fanning friction factor with HCT-Reynolds number at different nanoparticles concentrations ($T_{t,i} = 55\,^{\circ}C$): (*a*) $\delta = 0.1194$ and (*b*) $\delta = 0.0392$

number at the same coil curvature ratio. This can be returned to the effective secondary flow due to centrifugal force, which increases at higher Reynolds number.

The influence of HCT-side inlet temperature on the thermal performance of the heat exchanger is studied for $0\% \leq \varphi \leq 2\%$ and $0.0392 \leq \delta \leq 0.1194$. A sample of the results is presented in Fig. 8 for $\delta = 0.0472$ and 0.1194 at $\varphi = 1\%$.

For all tested heat exchangers, it is clear that as the HCT-side inlet temperature increases, $\overline{Nu}_t$ goes down at same Reynolds number. This can be attributed to the decrease in Prandtl number with increasing fluid temperature.

6.2 Pressure Drop Results. Experimental runs are carried out to investigate the effects of nanoparticles loading, coil curvature, and HCT-fluid inlet temperature on friction factor inside HCT. The nanoparticles volume concentration is varied from 0% to 2% and the HCT-volume flow rate is varied from 1.7to11.158l/min at coil inlet fluid temperature of 45 °C, 55 °C, and 65 °C. The corresponding dimensionless parameters are $5646 \leq Re_t \leq 54,018$ and $0.0392 \leq \delta \leq 0.1194$. Figure 9 presents a sample of the results for the effect of nanoparticles loading for $\delta = 0.1194$ and 0.0392 at $T_{t,i} = 55\,^{\circ}C$. Figure 10 shows a sample of the results for the effect of coil curvature ratio for $\varphi = 1\%$ at $T_{t,i} = 55\,^{\circ}C$.

It is seen from Fig. 9 that f_c of nanofluids is higher than that of the base fluid at same flow condition, and this increase goes up as φ increases. The average increase in f_c is of 4.1–7.1% at $\varphi = 0.5\%$ and of 25.7–27.4% at $\varphi = 2\%$ for $\delta = 0.1194$. While its corresponding average increase for $\delta = 0.0392$ is of 14.1–6.9% at $\varphi = 0.5\%$ and of 41.5–27.6% at $\varphi = 2\%$. This can be returned to high viscosity of the nanofluid, which increases with increasing the nanoparticles loading in the base fluid.

From Fig. 10, it can be seen that increasing the coil curvature ratio leads to significant increase in f_c at the same Re_t and $T_{t,i}$. The average increase in f_c is of 21.4–7.9% at $\varphi = 0.5\%$ and of

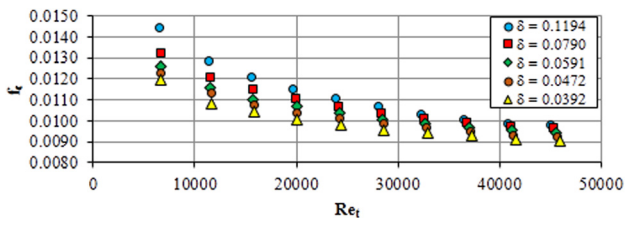

Fig. 10 Variation of HCT-fanning friction factor with HCT-Reynolds number at different HCT-curvature ratios ($\varphi = 1\%$, $T_{t,i} = 55\,^{\circ}C$)

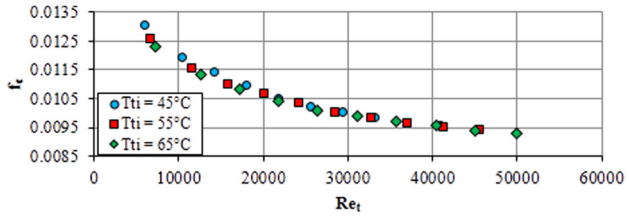

Fig. 11 Variation of HCT-fanning friction factor with HCT-Reynolds number at different HCT-inlet temperatures ($\varphi = 1\%$, $\delta = 0.0591$)

18.2–7.5% at $\varphi = 2\%$ when δ increases from 0.0392 to 0.1194. This can be attributed to the increase in the centrifugal force, which induces more effective secondary flow. Furthermore, Fig. 11 shows a sample of the results for the effect of HCT-side inlet temperature for $\varphi = 1\%, \delta = 0.0591$. It is clear that the effect of $T_{t,i}$ on f_c is nearly insignificant. This may be returned to the low effect of viscous force compared with the higher centrifugal force, which is the dominant at HCT-Reynolds number.

7 Thermal Performance Index (TPI)

To be a successful heat transfer fluid, the rise in convective heat transfer given by the nanofluid should be higher than the rise in pressure drop due to inclusion of nanoscale solid particles in the base fluid. The TPI is determined using $\bar{h}_t$ ratio and the pressure drop ratios that are calculated using the values obtained for γ-Al2O3 (40 nm)/water nanofluid and pure water, as follows [20]:

$$\text{TPI} = \frac{\bar{h}_{t,nf}/\bar{h}_{t,bf}}{\Delta P_{c,nf}/\Delta P_{c,bf}} \tag{22}$$

Over the studied range of HCT-Reynolds number, the average TPI was calculated and the results are illustrated at different HCT-side inlet temperatures in Fig. 12 for different coil curvature ratios and nanoparticles concentrations.

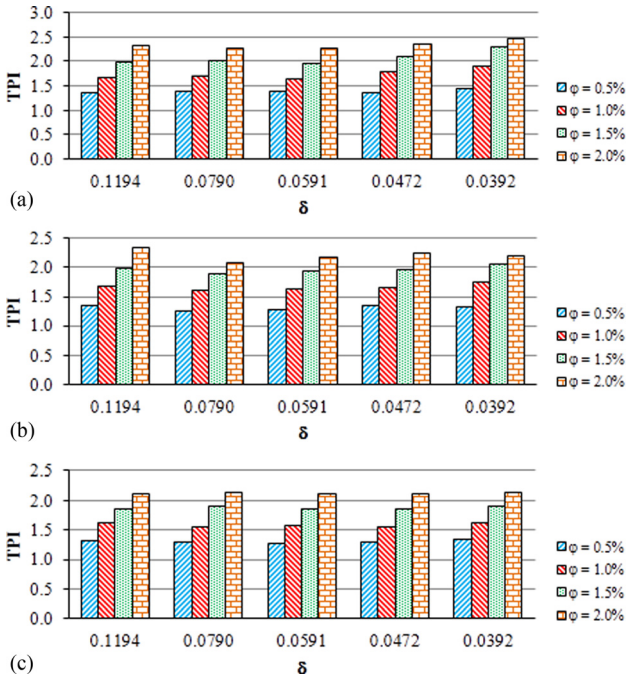

Fig. 12 Variation of the average TPI with HCT-curvature ratio at different nanoparticles concentrations: (*a*) $T_{t,i} = 65\,^{\circ}\text{C}$, (*b*) $T_{t,i} = 55\,^{\circ}\text{C}$, and (*c*) $T_{t,i} = 45\,^{\circ}\text{C}$

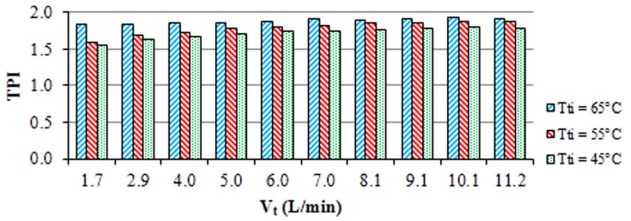

Fig. 13 Variation of the average TPI with HCT-volume flow rate at different nanoparticles concentrations

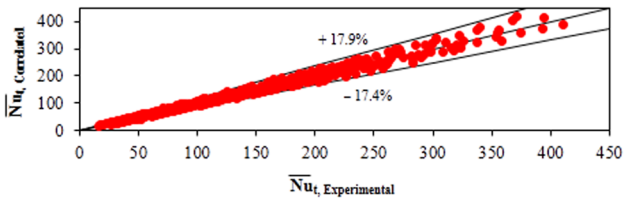

Fig. 14 Comparison of experimental values for HCT-average Nusselt number with that correlated by Eq. (23)

It obvious that the TPI is more than unity, which states that the enhancement in the heat transfer rate in the HCTs due to using nanofluids is higher than the corresponding increase in the pressure drop. This assures the ability of using γ-Al_2O_3 (40 nm)/water nanofluid in the HCTs with $0.5\% \leq \varphi \leq 2\%$ as a compound heat transfer enhancement technique inside shell and coil heat exchangers instead of using HCTs only. Moreover, it is shown for all HCTs that increasing φ enhances the TPI. Over the studied range of HCT-Reynolds number, the average value of TPI is of 1.33 and 2.23 at $\varphi = 0.5\%$ and $\varphi = 2\%$, respectively. Additionally, it is shown that the effect of coil curvature ratio is nearly insignificant on the TPI.

Furthermore, over the studied range of HCT-geometrical parameters and nanoparticles concentrations, the average TPI was calculated and the results are illustrated for different HCT-side flow rates in Fig. 13. From this figure, it is evident that increasing the HCT-side flow rate slightly enhances the TPI at lower flow rate, and this enhancement goes down as HCT-side flow rate increases. The average value of TPI is of 1.66 and 1.85 at $\dot{V}_t$ of 1.7 l/min and 11.16 l/min, respectively. Moreover, it is observed in Figs. 12 and 13 that increasing HCT-side inlet temperature slightly enhances the TPI. The average value of TPI is of 1.72–1.89 when $T_{t,i}$ varies from 45 °C to 65 °C, respectively.

8 Correlations for Coiled Tube-Average Nusselt Number and Fanning Friction Factor

Using the present experimental data, correlations were developed to predict the HCT-average Nusselt number and fanning friction factor. The HCT-average Nusselt number is correlated as a function of HCT Reynolds, Prandtl numbers, coil curvature ratio, and nanoparticles volume fraction

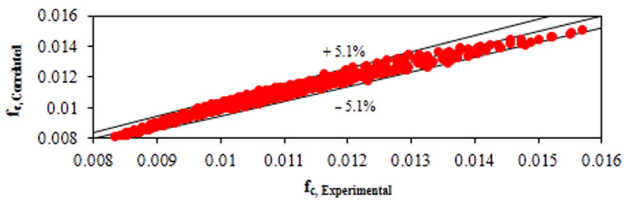

Fig. 15 Comparison of experimental values for HCT-fanning friction factor with that correlated by Eq. (24)

$$\overline{\mathrm{Nu}}_t = 0.0879\ \mathrm{Re}_t^{0.9833}\ \mathrm{Pr}_t^{1.7421}\delta^{0.5408}\varphi^{0.6376} \quad (23)$$

Equation (23) is applicable for $5702 \le \mathrm{Re}_t \le 55,101$, $1155 \le \mathrm{De}_t \le 18,669$, $1.92 \le \mathrm{Pr}_t \le 3.9$, $0.0392 \le \delta \le 0.1194$, and $0.005 \le \varphi \le 0.02$.

Another correlation was obtained for fanning friction factor in the HCT within $5646 \le \mathrm{Re}_t \le 54,018$, $1139 \le \mathrm{De}_t \le 18,267$, $0.0392 \le \delta \le 0.1194$, and $0.005 \le \varphi \le 0.02$

$$f_c = 0.12724\ \mathrm{Re}_t^{-0.1651}\delta^{0.0986}\varphi^{0.1204} \quad (24)$$

Comparisons of the present experimental HCT-average Nusselt number and fanning friction factor with those calculated by the proposed correlations are shown in Figs. 14 and 15. It is evident that the proposed correlations are in good agreement with the present experimental data. It is clearly seen that the data falls of the proposed equations within maximum deviation of $\pm 17.9\%$ and $\pm 5.1\%$ for $\overline{\mathrm{Nu}}_t$ and f_c, respectively.

9 Conclusions

The present work was carried out to investigate the heat transfer characteristics in shell and coil heat exchanger, in addition to the pressure drop inside the HCTs. The investigated ranges are $5702 \le \mathrm{Re}_t \le 55,101$, $1155 \le \mathrm{De}_t \le 18,669$, $1.92 \le \mathrm{Pr}_t \le 3.9$, $0.0392 \le \delta \le 0.1194$, and $0.005 \le \varphi \le 0.02$. From the study, it could be concluded that:

- For all HCT-geometric variables and operating conditions, utilization of γ-Al_2O_3 (40 nm)/water nanofluid with $\varphi \le 2\%$ instead of pure water in the HCTs results in remarkable heat transfer enhancement; this goes up as the nanoparticle concentration increases. This phenomenon was considered as an attribution to thermal conductivity enhancement and Brownian motion effect.
- For same operating conditions, the HCT-geometrical variables have a significant effect on the heat transfer. According to the experimental data, increasing the coil curvature ratio leads to augmenting the heat transfer rate of base fluids as well as nanofluids. This is because rapid developments of secondary flow enhance heat transfer.
- For all HCT-geometric variables, the operating conditions of the HCT-side affect directly on their thermal performance. For pure water as well as nanofluids experiments, the heat transfer rate goes up as the mass flow rate increases and as the fluid inlet temperature decreases. This is because rapid developments of secondary flow, turbulence level, and increasing Prandtl number enhance heat transfer.
- For all geometric variables and operating conditions, utilization of γ-Al_2O_3 (40 nm)/water nanofluid with $\varphi \le 2\%$ instead of pure water in the HCTs results in remarkable HCT-friction factor increase which goes up as the nanoparticle concentration increases. This is due to increasing nanofluid viscosity as the nanoparticles loading increases.
- For same operating conditions, the HCT-geometrical variables have a significant effect on the HCT-friction factor. According to the experimental data, increasing the coil curvature ratio leads to increase the HCT-friction factor for base fluids as well as nanofluids. This is because rapid developments of secondary flow.
- For all HCT-geometric variables, the effect of HCT-fluid inlet temperature on the HCT-friction factor is nearly insignificant. This can be attributed to the lower effect of viscosity variation compared with the centrifugal force.
- For all geometric variables and operating conditions, the TPI is more than unity, which states that the enhancement in the heat transfer rate in the HCTs due to using γ-Al_2O_3/water nanofluid is higher than the corresponding increase in the pressure drop. Therefore, this assures the ability of using γ-Al_2O_3 (40 nm)/water nanofluid in the HCTs with $\varphi \le 2\%$ as a compound heat transfer enhancement technique inside shell and coil heat exchangers instead of using HCTs only.
- The TPI increases with increasing nanoparticles concentration and HCT-side inlet temperature. Nevertheless, it is shown that the effect of coil curvature ratio is nearly insignificant.
- Correlations for the HCT-average Nusselt number and fanning friction factor as a function of the investigated parameters are obtained.

Nomenclature

A = area (m^2)
C_p = specific heat (J/kg °C)
d = diameter (m)
D = diameter (m)
f = fanning friction factor
h = average convection heat transfer coefficient (W/m^2 °C)
k = thermal conductivity (W/m °C)
L = length (m)
m = mass (kg)
$\dot{m}$ = mass flow rate (kg/s)
N = number of turns of the HCT
p = pitch of HCT (m)
P = pressure (Pa)
Q = heat transfer rate (W)
T = temperature (°C)
u = mean axial velocity (m/s)
U = overall heat transfer coefficient (W/m^2 °C)
V = volume (m^3)

Dimensionless Groups

De = Dean number, $\mathrm{Re}_t\delta^{0.5}$
$\overline{\mathrm{Nu}}$ = average Nusselt number
Pr = Prandtl number
Re = Reynolds number

Greek Symbols

γ = gamma
Γ = modeling function was introduced in Eq. (6)
δ = dimensionless coil curvature ratio, $d_{t,i}/D_c$
Δ = differential
$it\kappa$ = Boltzmann constant,1.3807×10^{-23} (J/K)
λ = dimensionless pitch ratio (coil torsion), $p_c/\pi D_c$
μ = dynamic viscosity (kg/ms)
ξ = modeling function was introduced in Eq. (6)
π = Pi ≡ a mathematical constant ≅ 3.1416
ρ = density (kg/m^3)
φ = nanoparticles volume concentration

Superscripts and Subscripts

ave = average
bf = base fluid
c = coil/contact
f = film/fluid/core flow
h = hydraulic
i = inner/inlet/internal
LM = logarithmic mean
m = mean
nf = nanofluid
np = nanoparticle
o = out/outer
s = surface
sh = shell
t = tube

Acronyms and Abbreviations

Al_2O_3 = alumina (aluminum oxide)
CuO = copper oxide
HCT = helically coiled tube
PVC = polyvinyl chloride
TiO_2 = titanium oxide
TPI = thermal performance index
vol. = volume
wt. = weight

References

[1] Choi, S. U. S., 1995, "Enhancing Thermal Conductivity of Fluid With Nanoparticles," *Developments and Applications of Non-Newtonian Flow*, ASME, New York, FED–Vol. 231/MD–Vol. 66, pp. 99–105.
[2] Li, Q., and Xuan, Y., 2002, "Convective Heat Transfer and Flow Characteristics of Cu–Water Nanofluid," Sci. China, Ser. E: Technol. Sci., **45**(4), pp. 408–416.
[3] Manca, O., Jaluria, Y., and Poulikakos, D., 2010, "Heat Transfer in Nanofluids," Adv. Mech. Eng., **2010**, p. 380826.
[4] Das, S. K., Choi, S. U. S., Yu, W., and Pradeep, T., 2007, *Nanofluids: Science and Technology*, Wiley, Hoboken, NJ.
[5] Pimenta, T. A., and Campos, J. B. L. M., 2012, "Friction Losses of Newtonian and Non-Newtonian Fluids Flowing in Laminar Regime in a Helical Coil," Exp. Therm. Fluid Sci., **36**, pp. 194–204.
[6] Gnielinski, V., 1986, "Heat Transfer and Pressure Drop in Helically Coiled Tubes," 8th International Heat Transfer Conference, San Francisco, CA, Vol. 6, pp. 2847–2854.
[7] Zhao, Z., Wang, X., Che, D., and Cao, Z., 2011, "Numerical Studies on Flow and Heat Transfer in Membrane Helical-Coil Heat Exchanger and Membrane Serpentine-Tube Heat Exchanger," Int. Commun. Heat Mass Transfer, **38**(9), pp. 1189–1194.
[8] Austin, L. R., and Seader, J. D., 1973, "Fully Developed Viscous Flow in Coiled Circular Pipes," AIChE J., **19**(1), pp. 85–94.
[9] Mishra, P., and Gupta, N., 1979, "Momentum Transfer in Curved Pipes. 1. Newtonian Fluids," Ind. Eng. Chem. Process Des. Dev., **18**(1), pp. 130–137.
[10] Prasad, B. V. S. S. S., Das, D. H., and Prabhakar, A. K., 1989, "Pressure Drop, Heat Transfer and Performance of a Helically Coiled Tubular Exchanger," Heat Recovery Syst. CHP, **9**(3), pp. 249–256.
[11] Ali, S., 2001, "Pressure Drop Correlations for Flow Through Regular Helical Coil Tubes," Fluid Dyn. Res., **28**(4), pp. 295–310.
[12] Rogers, G. F. C., and Mayhew, Y. R., 1964, "Heat Transfer and Pressure Loss in Helically Coiled Tubes With Turbulent Flow," Int. J. Heat Mass Transfer, **7**(11), pp. 1207–1216.
[13] Austen, D. S., and Soliman, H. M., 1988, "Laminar Flow and Heat Transfer in Helically Coiled Tubes With Substantial Pitch," Exp. Therm. Fluid Sci., **1**(2), pp. 183–194.
[14] Yang, G., Dong, F., and Ebadian, M. A., 1995, "Laminar Forced Convection in a Helicoidal Pipe With Finite Pitch," Int. J. Heat Mass Transfer, **38**(5), pp. 853–862.
[15] Yang, G., and Ebadian, M. A., 1996, "Turbulent Forced Convection in a Helicoidal Pipe With Substantial Pitch," Int. J. Heat Mass Transfer, **39**(10), pp. 2015–2022.
[16] Cengiz, Y., Yasar, B., and Dursun, P., 1997, "Heat Transfer and Pressure Drops in a Heat Exchanger With a Helical Pipe Containing Inside Springs," Energy Convers. Manage., **38**(6), pp. 619–624.
[17] Rahul, S., Gupta, S. K., and Subbarao, P. M. V., 1997, "An Experimental Study for Estimating Heat Transfer Coefficient From Coiled Tube Surfaces in Cross-Flow of Air," Proceedings of the Third ISHMT-ASME Heat and Mass Transfer Conference and Fourth National Heat and Mass Transfer Conference, Kanpur, India, Dec. 29–31, pp. 381–385.
[18] Kumar, K. P., Saibabu, J., Rao, K. V. N. S., and Srikanth, D. N., 2008, "Experimental Analysis of Sisal Nanofluids in Shell and Coil Heat Exchanger," Int. J. Nanosyst., **1**(1), pp. 87–90.
[19] Huminic, G., and Huminic, A., 2011, "Heat Transfer Characteristics in Double Tube Helical Heat Exchangers Using Nanofluids," Int. J. Heat Mass Transfer, **54**(19–20), pp. 4280–4287.
[20] Hashemi, S. M., and Akhavan-Behabadi, M. A., 2012, "An Empirical Study on Heat Transfer and Pressure Drop Characteristics of CuO–Base Oil Nanofluid Flow in a Horizontal Helically Coiled Tube Under Constant Heat Flux," Int. Commun. Heat Mass Transfer, **39**(1), pp. 144–151.
[21] Mukesh Kumar, P. C., Kumar, J., and Suresh, S., 2012, "Heat Transfer and Friction Factor Studies in Helically Coiled Tube Using Al_2O_3/Water Nanofluid," Eur. J. Sci. Res., **82**(2), pp. 161–172.
[22] Mukesh Kumar, P. C., Kumar, J., Suresh, S., and Praveen Babu, K., 2012, "Experimental Study on Parallel and Counter Flow Configuration of a Shell and Helically Coiled Tube Heat Exchanger Using Al_2O_3/Water Nanofluid," J. Mater. Environ. Sci., **3**(4), pp. 766–775.
[23] Mukesh Kumar, P. C., Kumar, J., Suresh, S., and Praveen Babu, K., 2012, "Heat Transfer Enhancement in a Helically Coiled Tube With Al_2O_3/Water Nanofluid Under Laminar Flow Condition," Eur. J. Sci. Res., **82**(2), pp. 161–172.
[24] Mukesh Kumar, P. C., Kumar, J., and Suresh, S., 2013, "Experimental Investigation on Convective Heat Transfer and Friction Factor in a Helically Coiled Tube With Al_2O_3/Water Nanofluid," J. Mech. Sci. Technol., **27**(1), pp. 239–245.
[25] Akbaridoust, F., Rakhsha, M., Abbassi, A., and Saffar-Avval, M., 2013, "Experimental and Numerical Investigation of Nanofluid Heat Transfer in Helically Coiled Tubes at Constant Wall Temperature Using Dispersion Model," Int. J. Heat Mass Transfer, **58**(1–2), pp. 480–491.
[26] Aly, W. I. A., 2014, "Numerical Study of Fluid Dynamic and Heat Transfer Performance of Nanofluid in Coiled Tube-in-Tube Heat Exchangers," Energy Convers. Manage., **79**, pp. 304–316.
[27] Elsayed, A., Al-dadah, R. K., Mahmoud, S., and Rezk, A., 2014, "Numerical Investigation of Turbulent Flow Heat Transfer and Pressure Drop of Al_2O_3/Water Nanofluid in Helically Coiled Tubes," Int. J. Low-Carbon Technol., **2014**, pp. 1–8.
[28] Kuppan, T., 2000, *Heat Exchanger Design Handbook*, Marcel Dekker, New York.
[29] Schmidt, E. F., 1967, "Heat Transfer and Pressure Loss in Spiral Tubes," Chem. Eng. Technol., **39**, pp. 781–789.
[30] Remsburg, R., 2001, *Thermal Design of Electronic Equipment* (Electronics Handbook Series), CRC Press, Boca Raton, FL.
[31] Koo, J., and Kleinstreuer, C., 2004, "A New Thermal Conductivity Model for Nanofluids," J. Nanopart. Res., **6**(6), pp. 577–588.
[32] Koo, J., and Kleinstreuer, C., 2005, "Laminar Nanofluid Flow in Microheat-Sinks," Int. J. Heat Mass Transfer, **48**(13), pp. 2652–2661.
[33] Pak, B. C., and Cho, Y., 1998, "Hydrodynamic and Heat Transfer Study of Dispersed Fluids With Submicron Metallic Oxide Particles," Exp. Heat Transfer, **11**(2), pp. 151–170.
[34] Xuan, Y., and Roetzel, W., 2000, "Conceptions for Heat Transfer Correlation of Nanofluids," Int. J. Heat Mass Transfer, **43**(19), pp. 3701–3707.
[35] Daily, J. W., and Harleman, D. R., 1966, *Fluid Dynamics*, Addison-Wesley, Don Mills, ON, Canada.
[36] Nigam, K. D. P., Agarwal, S., and Srivastava, V. K., 2001, "Laminar Convection of Non-Newtonian Fluids in the Thermal Entrance Region of Coiled Circular Tubes," Chem. Eng. J., **84**(3), pp. 223–237.
[37] Kline, S. J., and McClintock, F. A., 1953, "Describing Uncertainties in Single-Sample Experiments," Mech. Eng., **75**(1), pp. 3–8.
[38] Xin, R. C., and Ebadian, M. A., 1997, "The Effects of Prandtl Numbers on Local and Average Convective Heat Transfer Characteristics in Helical Pipes," ASME J. Heat Transfer, **119**(3), pp. 467–473.
[39] White, C. M., 1932, "Friction Factor and Its Relation to Heat Transfer," Trans. Inst. Chem. Eng., **18**, pp. 66–86.